석 사 학 위 논 문
Master's Thesis

신기루 영상 제작의 직관적 편집

Artistic Editing for Mirage Image Generation

2017

최 병 윤 (崔 炳 允 Choi, Byungyoon)

한 국 과 학 기 술 원

Korea Advanced Institute of Science and Technology

석 사 학 위 논 문

신기루 영상 제작의 직관적 편집

2017

최 병 윤

한 국 과 학 기 술 원

전산학부

신기루 영상 제작의 직관적 편집

최 병 윤

위 논문은 한국과학기술원 석사학위논문으로
학위논문 심사위원회의 심사를 통과하였음

2016년 12월 19일

심사위원장 윤 성 의 (인)

심 사 위 원 김 민 혁 (인)

심 사 위 원 이 기 혁 (인)

Artistic Editing for Mirage Image Generation

Byungyoon Choi

Advisor: Sung-eui Yoon

A dissertation submitted to the faculty of
Korea Advanced Institute of Science and Technology in
partial fulfillment of the requirements for the degree of
Master of Science in Computer Science

Daejeon, Korea
2016, December

Approved by

Sung-eui Yoon
Associate Professor of Computer Science

The study was conducted in accordance with Code of Research Ethics[1].

[1] Declaration of Ethical Conduct in Research: I, as a graduate student of Korea Advanced Institute of Science and Technology, hereby declare that I have not committed any act that may damage the credibility of my research. This includes, but is not limited to, falsification, thesis written by someone else, distortion of research findings, and plagiarism. I confirm that my thesis contains honest conclusions based on my own careful research under the guidance of my advisor.

MCS 20153639

최병윤. 신기루 영상 제작의 직관적 편집. 전산학부 . 2017년. 22+ii 쪽. 지도교수: 윤성의. (영문 논문)

Byungyoon Choi. Artistic Editing for Mirage Image Generation. School of Computing . 2017. 22+ii pages. Advisor: Sung-eui Yoon. (Text in English)

초 록

이 논문에서는 신기루 영상을 제작할 때 필요한 직관적인 인터페이스를 소개한다. 신기루가 포함된 영상을 제작할 때 더 직관적인 편집을 할 수 있도록 하는 방안을 제시하였다. 이를 만족하기 위해 두 중요한 개념을 사용한다. 첫째는 시작점-도착점 쌍으로써, 사용자가 신기루의 상의 본이 될 물체의 위치와 그 물체의 신기루가 생길 위치를 직관적으로 설정할 수 있게 해 준다. 둘째는 스칼라 장의 매개변수표현으로써, 신기루 현상을 물리적으로 만들어 내는 개념인 공간상에서의 굴절률을 효과적으로 표현할 수 있게 해 준다. 이 논문에서는 사용자 입력을 만족시키는 굴절률의 공간 분포를 찾기 위해 매개변수공간 상에서 최적화를 수행한다. 최적화 결과가 실제로 사용자가 입력한 원하는 결과인지를 시각적으로 보임으로써 이 방법이 맞다는 것을 보인다.

핵 심 낱 말 직관적 편집, 사용자 인터페이스, 비선형 렌더링, 신기루

Abstract

This paper presents an intuitive user interface for generating the rendered image of a mirage. The proposed interface focuses on providing better artistic control over the production of a mirage scene. Our method utilizes two core concepts to do so. The first idea, Source-to-Destination Point Pair, presents an intuitive way to designate the relationship between a source position of an object and its destination position of the mirage effect. The second idea, Parametric Representation of a Scalar Field, enables us to effectively represent a spatial distribution of a refractive index, which physically controls the mirage effect in a compact form. We perform an optimization on this parameter space to find the spatial distribution of the refractive index satisfying the user input. We validate the method visually by comparing whether the resulting image agrees with a goal state given by a user.

Keywords artistic control, user interface, non-linear rendering, mirage

Contents

Contents . . . .
List of Tables i
List of Figures ii

Chapter 1. Introduction **1**

Chapter 2. Related Works **2**
- 2.1 Modeling Refractive Index Distribution 2
- 2.2 Rendering with Continuous Refraction 2
- 2.3 Artistic Editing 3

Chapter 3. Background **4**
- 3.1 Physical Background of the Mirage Image 4
- 3.2 Artistic Editing of the Mirage Image 4

Chapter 4. User Interface and Optimization **7**
- 4.1 Source-to-Destination Point Pair 7
- 4.2 Spatial Encoding and Optimization 7
- 4.3 Finding Appropriate Parametric Representation 8

Chapter 5. Implementation **13**

Chapter 6. Results **14**
- 6.1 Optimization Time 14
- 6.2 Optimization and Rendering Results 14

Chapter 7. Conclusion, Limitation and Future Work **19**

Bibliography **20**

Acknowledgments in Korean **22**

List of Tables

4.1 Symbols used for the paper 8
4.2 Symbols used in the temperature formulation (Eq. 4.2) 9
4.3 Symbols used in our refractive index formulation (Eq. 4.3) 10

6.1 Legend for the markers in the screenshots 14

List of Figures

3.1 Mirages are classified based on its relative location to its original object. Image courtesy of Ludovica Lorenzelli. . . . 5
3.2 An example of different mirage classes. Image courtesy of Conjecture Corporation for (a), Shawn Stockman-Malone for (b). . . . 5
3.3 Various mirage photographs for the same location with the different distortion. All of the photographs are superior mirage, but the difference in distortion makes the difference in the look and feel. Notice the difference in the green ellipse. Image courtesy of Pekka Parviainen. . . . 6

4.1 This shows the relationship between Source-to-Destination Point Pair and the artistic aspects of the mirage effect. . . . 11
4.2 This shows a trend plot of refractive index distribution created by our model (Eq. 4.3) along with the original APM. We can visually find the similarity between trend plots of our model and APM. . . . 12

6.1 This shows the relationship between the number of Source-to-Destination Point Pairs and the time spent on optimization. . . . 15
6.2 User input, light traces, and the rendered effect for a superior mirage in a 3D scene. User input is shown as marker; the blue plus (+) represents the destination point, and the orange square (□) represents the source point. The light traces acquired from the computed refractive index by the optimization is the visualized as the yellow curves, while the skyblue lines represent the line of sight; see Table 6.1 for the legend. The rightmost figure shows the computed mirage effect given the user input. . . . 16
6.3 The image (a) show user inputs, while the image (b) shows trace of lights. The image (c) shows the computed, inferior mirage effect. . . . 16
6.4 The image (a) show user inputs, while the image (b) shows trace of lights. The image (c) shows the rendered inferior mirage effect. This one shows different distortion state compared to that of Figure 6.3. . . . 17
6.5 The image of the scene sharing the same refractive index settings as Figure 6.2. The image shows that the user can navigate through space with the consistent refractive index distribution. . . . 17
6.6 This shows a 2D application for two different mirage types on 2D geometry. Our method can be easily applied to 2D scenes without any changes. . . . 18

Chapter 1. Introduction

Rendering the meteorological optical phenomena has been studied, because of its frequent observations around our daily lives and its ability to convey different mood through its visual aspects. Those phenomena, e.g. the sky reflected on roads in a hot and sunny day, are thus used in visual effects for various media such as movies.

While having an importance as a visual effect, only a few attempts have been made in a study of providing an artistic control over such effects. It is especially difficult to find works about the effects of complex light propagation like a mirage. Due to the nonlinearity of the light trails in the mirage effect, the conventional techniques dealing with a straight light trace cannot work well when providing artistic control for those effects.

The nonlinearity of light paths for the mirage effect is caused by the varying refractive index of the air, which acts as the light media. Therefore, controlling the mirage as the visual effect requires better understandings about the distribution of the index of refraction in the light media. It is also critical to provide an intuitive artistic control for editing visual effects accompanying nonlinear light paths.

Main contributions. To enable intuitive controls on editing the mirage effects, we propose a simple user interaction scheme based on source-to-destination point pairs. A user specifies a target object as a source point, while the destination point designates the desired position of a mirage image of the target object. Given this user input, we propose an optimization scheme and compact representation of a spatial distribution of refractive index. To demonstrate representation power and usability of our approach, we have applied our method to generate different types of mirage effects and verify visually.

While we consider only a particular effect of meteorological optical phenomena, we believe that we take a meaning step to providing artistic controls on complex optical effects.

Chapter 2. Related Works

Controlling a visual effect of mirage tackles multiple problems. These problems include how to model a refractive index distribution, how to render the scene with a light media with continuously differing refractive index and the artistic editing with nonlinear light paths. We discuss related works on these topics in this section.

2.1 Modeling Refractive Index Distribution

Handling light effects undergoing a continuous refraction requires a modeling of the spatial distribution of the refractive index. Those models are designed and chosen often based on their applications, such as the reconstruction of the atmosphere status or the optical simulation of the heat transfer.

There is the simplest approximation on the air with continuously differing refractive index along the height, namely a *series of air layer*. It considers the whole air as the series of discontinuous air layers with different constant optical densities [1]. This simple model was suggested as the proof-of-concept of the new approach to the mirage rendering. The approximation was used because the precise rendering requires the nonlinear ray tracing, yet not available at that moment. While simple to calculate, it produces less than satisfying quality given the standard to be used in the industry.

There is another representation of the atmosphere based on U.S. standard atmosphere 1976 with systematized modifications. Gutierrez et al. [2] introduced this model for the simulation of the atmospheric phenomena, such as a mirage. This model uses the Earth's atmosphere profile as its base since this application focuses on the reproduction of the actual various atmospheric phenomena. Because of this, this model has a difference of the refractive index along the altitude only.

There also exist a model, namely *heat transfer simulation*, representing air heated from the hot spots [3]. The spatial distribution of the refractive index is calculated by simulating the heat transfer in the given system. This representation is used to render another optical phenomenon, a heat shimmering.

As shown in these cases, one should use the fittest model of the refractive index for every application among the various to simplify the representation and thus calculation. We introduce a new model which is appropriate to our goal in this research.

2.2 Rendering with Continuous Refraction

Rendering a mirage image requires the calculation of curved light path created due to the continuous refraction.

Ament et al. [4] developed a new radiative transfer equation which takes refraction into consideration – refractive radiative transfer. They also came up with the new rendering equation with continuously refracted light rays. This new rendering equation produces physically correct light paths and conserves energy through the radiation transfer.

There have been several kinds of research utilizing the rendering equation derived from the refractive radiative transfer. Some of them include an application-specific inverse rendering problem in medical imaging [5] or an optics simulation in designing better lens system [6]. Our work also utilizes the rendering equation for our problem.

There have been several other previous different approaches to calculating curved light paths. Including the very first trial on rendering a mirage image [1], multiple instances of Snell's law have been used for the discontinuous-air-layer models. There was another approach utilizing a Fermat's principle taking a continuous refraction into consideration, rather than approximating it into multiple discontinuous refractions on dielectric planes [2].

2.3 Artistic Editing

Artistic editing is the field of study whose goal is to support artists to effectively design rendered image's appearance to "convey an explicit mood or information" [7]. Such study focuses on providing artists more controls on their appearance design by improving the intuition of the editing session. The improvement of the intuition has various methodologies to achieve, and most of them work on improving the predictability – making the artists/designers to predict the rendering results better, while they are editing the scene.

Nonlinear Light. As an example of an artistic editing with nonlinear light paths, there is a work by Kerr et al. [8] on editing direct illumination by curving light rays. They provided a system to let users to 'bend' the light rays by reshaping splines. That is, the user edits the guide spline's shape to directly define how the light will be curved. Our research also works with the curved light rays but in different ways.

Atmospheric Effect. For example of an atmospheric effect, there is a study on the appearance design of the volume [9]. This research optimized physically-based properties of the volume based on the provided user input, describing the desired rendering image of the volume. This method also provided a decent interface to edit a volume, which was previously difficult to do in an efficient manner. Our paper suggests a similar system for another atmospheric effect, a mirage.

User Interface. Finally, there is work on artistic editing utilizing similar user interface as this paper suggests. Research by Ritschel et al. [10] proposes a user interface to interactively and intuitively edit the reflections. They utilize a set of pairs of points(or 'handles') as user-defined constraints. It is related to our work because we also use similar user constraint, but with different semantics.

Chapter 3. Background

Since we are working on a visual expression based on actual phenomena, studying a physical nature of the phenomena is important. In this section, we explain the physical background of a meteorological optical phenomenon, especially mirage (Sec. 3.1). Alongside with the scientific description, we research which aspect should be emphasized during an artistic editing (Sec. 3.2).

3.1 Physical Background of the Mirage Image

A mirage is an optical phenomenon produced by light refracted during traveling through the air. The atmosphere is an inhomogeneous light medium, that is, its physical properties such as temperature and pressure differ continuously along the spatial dimensions. The difference in air temperature and pressure results in varying refractive index of the medium, because the index of refraction depends on the density of the media [11]. This continuously varying refractive index affects the light path getting through.

A specific spatial distribution of refractive indices of the medium produces nonlinear light paths due to consecutive refractions. This nonlinear light trail terminates on the observer's eye. Since the observer presumably assumes the light to travel in a linear manner, one will perceive a displaced image of an object. The image may also be distorted because all light paths reflected from the object are not necessarily aligned, especially when lights travel through non-homogeneous light media. This displaced, distorted image formed by nonlinear light traces is called a mirage image.

3.2 Artistic Editing of the Mirage Image

In this section, we focus on the mirage image creation in an artistic point of view rather than discussing how it occurs in nature. To consider a mirage as an artistic expression, we formulate the artistic aspects of this optical phenomenon.

We may regard some visual factor as the artistic aspect if it has high visual prominence in a particular artistic expression [7]. Hence, it is required to observe various pieces of art using such expression for a proper formulation. Inspecting numerous photographs of a mirage gives an observation that a position of a mirage image is one of the significant visual elements. We can infer the significance of a relative location of a mirage to the original object from the fact that it is one of the criteria of mirage classification (see Figure 3.1 and Figure 3.2).

Another axis of the visual aspects of the phenomena is a distortion of an image. The way how a distortion shapes the refracted image necessarily changes a mood conveyed to viewers of a mirage picture (see Figure 3.3). In this work, we focus on two visual characteristics, a position and distortion shape, to design an effective user interface for an artistic editing of the mirage image creation.

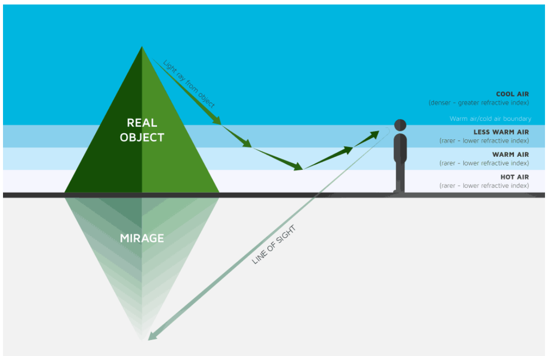

(a) Inferior mirage illustration.

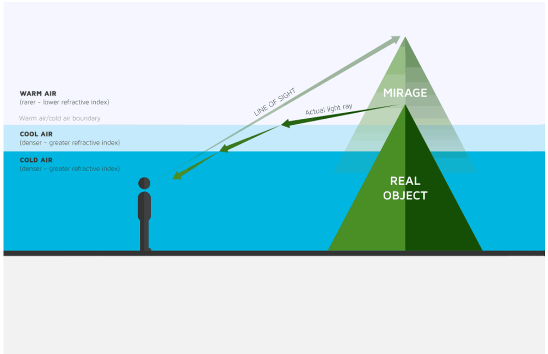

(b) Superior mirage illustration.

Figure 3.1: Mirages are classified based on its relative location to its original object. Image courtesy of Ludovica Lorenzelli.

(a) A photograph of inferior mirage on the hot road.

(b) A photograph of superior mirage on the cold ocean.

Figure 3.2: An example of different mirage classes. Image courtesy of Conjecture Corporation for (a), Shawn Stockman-Malone for (b).

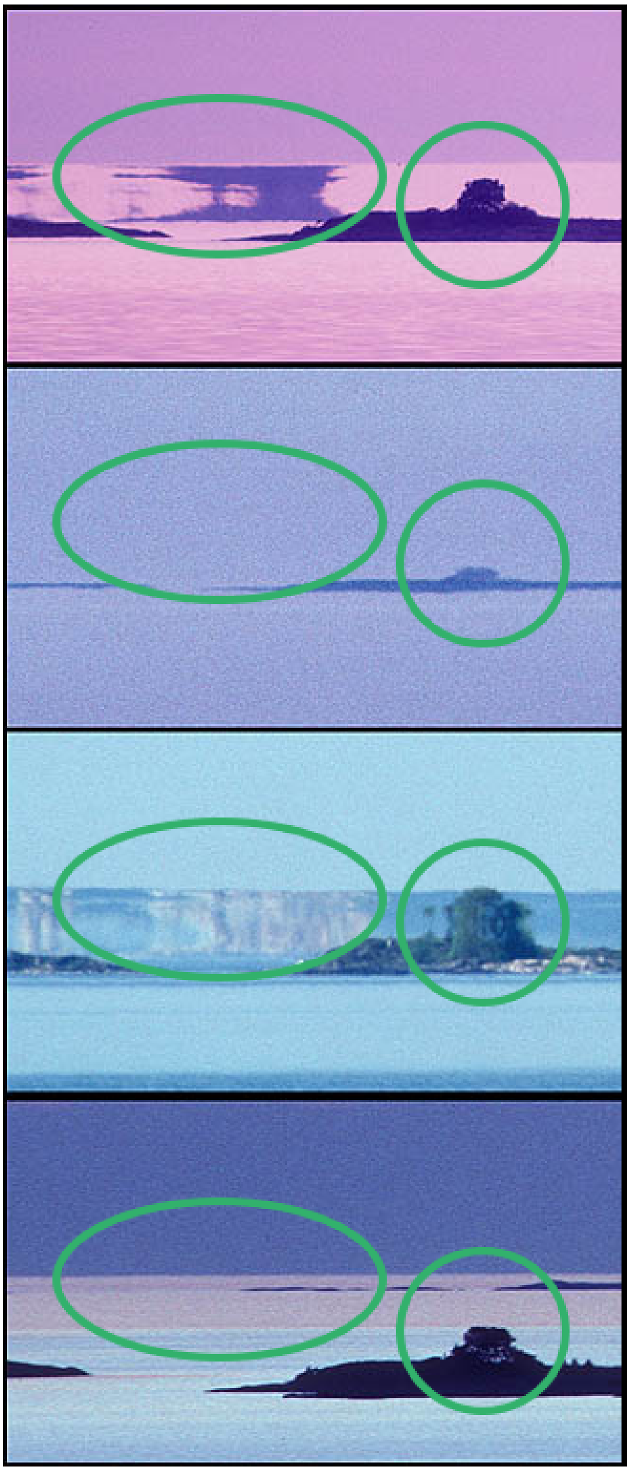

Figure 3.3: Various mirage photographs for the same location with the different distortion. All of the photographs are superior mirage, but the difference in distortion makes the difference in the look and feel. Notice the difference in the green ellipse. Image courtesy of Pekka Parviainen.

Chapter 4. User Interface and Optimization

It is often needed to design a customized human-computer interaction scheme to provide better control of the artistic editing session. In this section, we discuss a user interface to assist the appearance editing and rationales behind our choices.

Task Definition. The task we focus on achieving in this research is to provide the better intuition during an appearance editing of a mirage image. We suppose that the artist has a goal state of the mirage effect. We define a goal state by distinct artistic aspects – position and distortion – which are set by the artist. Before elaborating our method, we summarize the symbols used in the rest of the paper in Table 4.1.

4.1 Source-to-Destination Point Pair

The position and the form of distortion of a displaced image are visually prominent factors for the mirage image. To provide an intuitive control on such visual factors, we utilize the concept of **Source-to-Destination Point Pair**s.

The pair of points, $(\boldsymbol{x}_{\mathrm{src}}, \boldsymbol{x}_{\mathrm{dst}})$, designates how should a light path be curved. It is consisted of a source point, $\boldsymbol{x}_{\mathrm{src}}$, and its destination point, $\boldsymbol{x}_{\mathrm{dst}}$. By setting these two points, the user can add a constraint to define a goal state. The constraint is that the light starting from the camera to $\boldsymbol{x}_{\mathrm{dst}}$ should be curved to hit the position $\boldsymbol{x}_{\mathrm{src}}$. In other words, it shows that the user wants a mirage image of an object at the location $\boldsymbol{x}_{\mathrm{src}}$ to appear at the location $\boldsymbol{x}_{\mathrm{dst}}$ (see Figure 4.1a).

Our work also utilizes more than one point pairs to allow users to specify the visual factors of mirage more precisely. Using multiple pairs of points allows a user to define one's desired distortion shape along with its position (see Figure 4.1b).

4.2 Spatial Encoding and Optimization

We then introduce a parametric representation to encode a scalar field of the refractive index. Let an m-dimensional parametric representation of a scalar field with a parameter $\boldsymbol{k} \in \mathbb{R}^m$ to be $L(\boldsymbol{k})$. We then define a spatial distribution of a refractive index which only depend to the parameter vector $\boldsymbol{k}$ to be $n_{L(\boldsymbol{k})} := L(\boldsymbol{k})$.

We have the Refractive Radiative Transfer Equation for the steady-state scene given by Ament et al. [4]:

$$\frac{d\boldsymbol{v}}{ds} = \nabla_{\boldsymbol{x}} n,$$
$$\frac{d\boldsymbol{x}}{ds} = \frac{\boldsymbol{v}}{n}.$$

This indicates that we can calculate the curved light path numerically from specific initial values given for the position $\boldsymbol{x}$ and velocity $\boldsymbol{v}$. We denote such initial values as $\boldsymbol{x}_0$ and $\boldsymbol{v}_0$.

Suppose that a user specifies a set of Source-to-Destination Point Pairs, each of which is denoted by $(\boldsymbol{x}_{\mathrm{src}_i}, \boldsymbol{x}_{\mathrm{dst}_i})$. Under the parametric representation of a refractive index $n_{L(\boldsymbol{k})}$, we think of the light path calculated by letting the initial values to be $\boldsymbol{x}_0 = \boldsymbol{x}_{\mathrm{cam}}$ and $\boldsymbol{v}_0 = (\boldsymbol{x}_{\mathrm{dst}_i} - \boldsymbol{x}_{\mathrm{cam}})/\|\boldsymbol{x}_{\mathrm{dst}_i} - \boldsymbol{x}_{\mathrm{cam}}\|$ for

Symbol	Description
$\boldsymbol{x}$, $\boldsymbol{x}_{\text{src/dst}}$, $\boldsymbol{x}_{\text{src/dst}_i}$	Position, of a source/destination, of an i-th point pair
$\boldsymbol{x}_{\text{cam}}$	Position of a camera
$\boldsymbol{v}$	Velocity of a light in medium
s, $s_{0/\max}$	Arc length, initial/maximum value
ds	Curved line element of the light path
$\boldsymbol{k}$	Parameter vector in m-dimension
$L(\boldsymbol{k})$	m-dimensional parametric representation of 3D scalar field
n, $n_{L(\boldsymbol{k})}$	Spatial distribution of a refractive index, defined by a parametric representation L and a parameter vector $\boldsymbol{k}$
$\boldsymbol{x}^*(s)$	Numerically calculated light path depending on the arc length s
ρ	Density of the air
T	Temperature of the air
h	Altitude

Table 4.1: Symbols used for the paper

the i-th point pair. The magnitude of an initial velocity is not relative here because a trace of a light refracted is dependent only to spatial location and radial unit vector of propagation of light [12]. We thus use a unit magnitude for the initial velocity, which is beneficial for consistent light path calculation.

We denote such light path to be $\boldsymbol{x}^*_{L(\boldsymbol{k}),i}(s)$ depending on the arc length s. Assume the computation of the light path have been done within the arc length domain of $[s_0, s_{\max}]$. We define the distance, $\text{dist}_{L,i}(\boldsymbol{k})$, between the path and the source point as the following:

$$\text{dist}_{L,i}(\boldsymbol{k}) := \inf\{\|\boldsymbol{x}^*_{L(\boldsymbol{k}),i}(s) - \boldsymbol{x}_{\text{src}_i}\| : s \in [s_0, s_{\max}]\}. \tag{4.1}$$

Our goal is then to find the parameter $\boldsymbol{k}$ that minimizes the cost function, $\text{cost}(\boldsymbol{k})$, summing the distance from each source point to its computed light path:

$$\text{cost}(\boldsymbol{k}) := \sum_i \text{dist}_{L,i}(\boldsymbol{k})$$

Among possible approaches to solve the problem, we take the parametric regression for computing the parameter vector $\boldsymbol{k}$.

4.3 Finding Appropriate Parametric Representation

While any parametric scalar field representation can be used as a refractive index encoder, we suggest an appropriate parametric representation (or 'model' for short) that can be useful for the effective mirage image generation.

Our approach starts with investigating the actual refractive index distribution of the atmosphere. Gutierrez et al. [2] have done an extensive study on the earth's atmosphere and its deviation that makes meteorological optical phenomena, including mirage. This approach came up with Atmospheric Profile Manager (APM), which is a tool providing parametric controls to adjust the atmospheric conditions. This tool is derived based on 1976 U.S. Standard Atmosphere model along with a parametric model of temperature versus altitude to de-standardize the air.

Symbol	Description
T_0	Temperature at altitude 0
r_T	Change rate of temperture along with altitude
$\Delta T_{\text{inv/hotspot}}$	Temperature difference occurred by inversion layer/hot spot
$h_{\text{ciso/hotspot}}$	Height of inversion layer/hot spot
a	Diffuseness of inversion layer
d_0	Dropoff length for hot spot

Table 4.2: Symbols used in the temperature formulation (Eq. 4.2)

This approach models three different atmospheric phenomena – inversion layers, hot spots, and noise grids – for the de-standardization. In short, inversion layers model an inverted temperature gradient along altitude, hot spots describe a temperature deviation caused by heat transferred from a certain position, and noise grids simulate a simplified version of the heat shimmering effect. We investigated a refractive index distribution created by this tool, excluding noise grids, because it is not necessary for our mirage image generation. By summing up the temperature models for U.S. Standard Atmosphere and de-standardizations, we get the following formulation of the temperature:

$$\begin{aligned} T(h) &= T_0 + r_T h && \text{U.S. Std. Atm.} \\ &+ \frac{\Delta T_{\text{inv}}}{1 + \mathrm{e}^{(h-h_{\text{ciso}})/a}} - \Delta T_{\text{inv}} && \text{Inversion Layer} \\ &+ \Delta T_{\text{hotspot}} \mathrm{e}^{-(h-h_{\text{hotspot}})/d_0}. && \text{Hot Spot} \end{aligned} \tag{4.2}$$

Symbols used in this formulation is summarized in Table 4.2.

Assuming a constant pressure along the altitude, the ideal gas law, $\rho \propto T^{-1}$, and a constant refractive index along a light wavelength, the Gladstone-Dale formula [11] shows that $n = \rho \cdot (n_{\text{avg}} - 1) + 1$, where n_{avg} is the average refractive index over visible wavelength. Assigning proper values to the parameters for an ease of investigation, we compute a plot of refractive index versus altitude.

By examining the plot, we have observed two important properties of the refractive index distribution. First, the value increases as the altitude go up without any de-standardization. Second, the de-standardizations cause the noticeable drops in value; higher change rate for the hot spot observed at the lower altitude, and an inverted gradient for the inversion layer which is located higher.

We, however, found that it is inappropriate to directly use this refractive index distribution model as the parametric representation for our problem. The U.S. Standard Atmosphere term includes a linear term, while $n \propto \rho \propto T^{-1}$. This results in the divergence of the value in certain altitude, because in certain altitude such term will hit the value of zero.

Instead of using the prior model of APM, we suggest a suitable parametric representation, namely **Logistic Approximation**. This model relies on a different formulation but follows notable trends of APM without having identified issues for our problem. Our parametric representation models all the properties using logistic functions, whose symbols are summarized in Table 4.3:

Symbol	Description
$n_{\mathrm{bg/inv/hotspot}}$	Refractive index difference caused by background/inversion layer/hot spot
h_{ciso}	Height of inversion layer
$a_{\mathrm{bg/inv/hotspot}}$	Rate of change of refractive index for background/inversion layer/hot spot
k_{s}	Scale factor

Table 4.3: Symbols used in our refractive index formulation (Eq. 4.3)

$$\begin{aligned} n(h) = & \frac{k_{\mathrm{s}}}{|n_{\mathrm{bg}}| + |n_{\mathrm{inv}}| + |n_{\mathrm{hotspot}}|} && \text{Normalize \& Scale} \\ & \cdot \Big(f_{\mathrm{logistic}}(n_{\mathrm{bg}}, a_{\mathrm{bg}}, 0, h) && \text{Background} \\ & + f_{\mathrm{logistic}}(n_{\mathrm{inv}}, -a_{\mathrm{inv}}, h_{\mathrm{ciso}}, h) && \text{Inversion Layer} \\ & + f_{\mathrm{logistic}}(n_{\mathrm{hotspot}}, a_{\mathrm{hotspot}}, 0, h) \Big) && \text{Hot Spot} \\ & + 1, && \text{Baseline} \end{aligned} \tag{4.3}$$

where

$$f_{\mathrm{logistic}}(L, k, x_0, x) := \frac{L}{1 + \mathrm{e}^{(x_0 - x)/k}}.$$

Logistic terms represent the difference in the refractive index along the altitude for background, inversion layer, and hot spot, respectively. The background changes, which correspond to the temperature change in U.S. Standard Atmosphere, have also been modeled using a logistic function to prevent the divergence. The sum of logistic terms is divided by the sum of their maximum values, to normalize the changes in the refractive index. The scale factor is utilized to adjust the actual amount that the refractive index deviates from the baseline value of 1. The plot of this formula visually confirms that this model reflects the essential properties of the refractive index distribution of APM, while suitable to our work (see Figure 4.2 for the trend plot).

The parameter vector of our representation is in the eight dimensional space:

$$\boldsymbol{k} = \begin{bmatrix} n_{\mathrm{bg}} & n_{\mathrm{inv}} & n_{\mathrm{hotspot}} & h_{\mathrm{ciso}} & a_{\mathrm{bg}} & a_{\mathrm{inv}} & a_{\mathrm{hotspot}} & k_{\mathrm{s}} \end{bmatrix}^T.$$

The role of each parameter can be differentiated despite of their similar forms by multiplying different constant weights to them, i.e., regularizing the parameters. For example, a_{bg} should be much larger than other rate-of-change parameters, because the background change should be much slower than the changes by other causes. One can reflect this behavior by multiplying larger constant weights than the others.

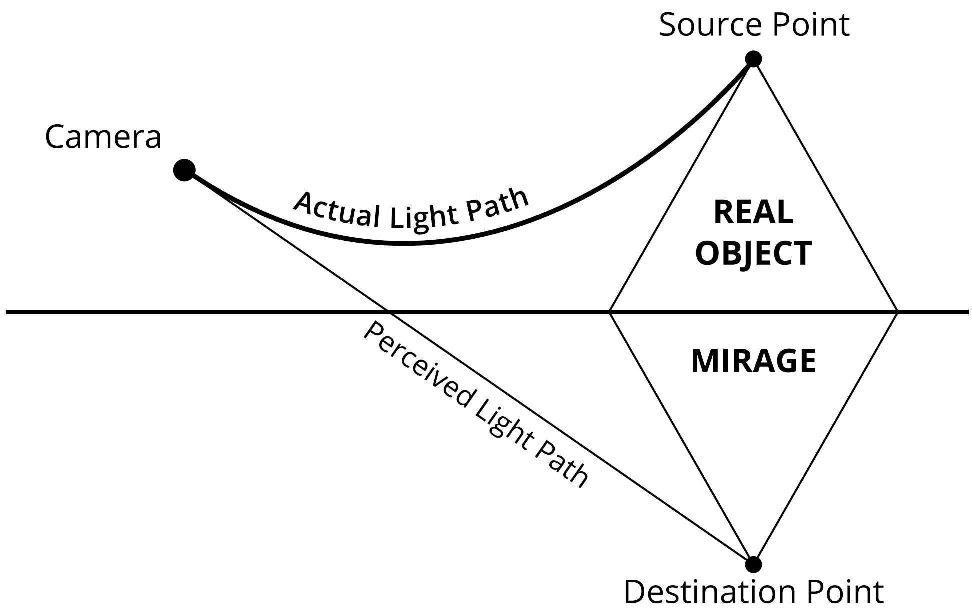

(a) This shows a basic role of a pair of source and destination points to specify a position of a mirage.

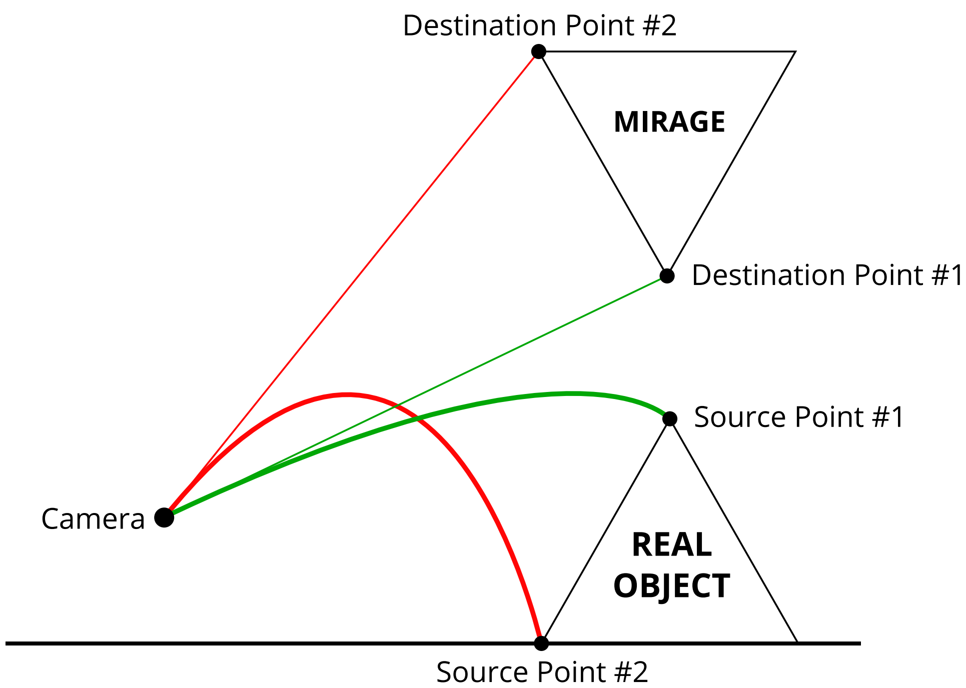

(b) Using multiple pairs of points on a single object can describe a distortion of a target mirage effect.

Figure 4.1: This shows the relationship between Source-to-Destination Point Pair and the artistic aspects of the mirage effect.

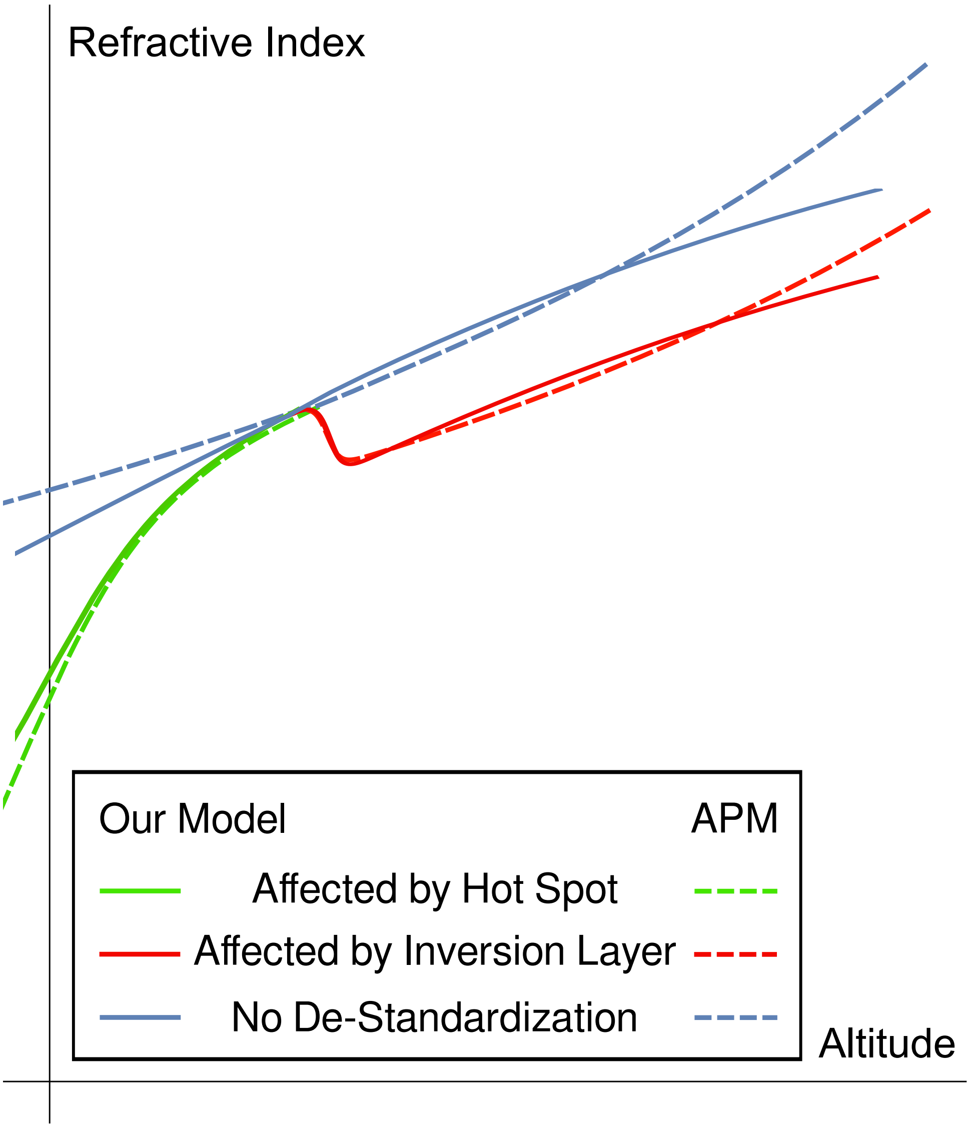

Figure 4.2: This shows a trend plot of refractive index distribution created by our model (Eq. 4.3) along with the original APM. We can visually find the similarity between trend plots of our model and APM.

Chapter 5. Implementation

We implemented the user interface to give a user control over a camera and Source-to-Destination Point Pairs. A user can manipulate the viewing camera in common keyboard and mouse interactions.

Once done on setting a camera, a user can proceed to the next phase of Source-to-Destination Point Pair setting or 'point pair setting' in short. In point pair setting, a user can place a new point by clicking on the viewport. By clicking on the viewport, our system computes the intersection between meshes in the scene and the ray starting from a camera in the direction of the mouse pointer. If there is an intersection, the location of the point is set to the location of the intersection. Starting from a destination point, a user can move on to the next subphase to put a corresponding source point by pressing a keystroke. After setting two points for a pair, a user may add another pair of points or press another key to finalize the point pair setting. When the point pairs are set, our system performs an optimization to compute the parameters for our representations of the spatial distribution of the refractive index.

The weight for the model's parameters in our implementation are the following: 10 for a_{bg}, 0.1 for a_{inv}, 0.3 for a_{hotspot}, and 0.003 for k_{s}. The weight have been multiplied to those parameters both during the optimization and rendering.

Since a term $\boldsymbol{x}^*_{L(\boldsymbol{k}),i}(s)$ in the cost function (Eq. 4.1) contains a numerically calculated variable, it is not available to have an analytic derivative of the cost function. We, therefore, utilized a derivative-free optimizer BOBYQA [13] for the optimization. We chose BOBYQA over other derivative-free optimization methods because it showed higher convergence rate than other algorithms even for a large number of variables for nonconvex smooth problems like ours [14].

We implemented a renderer for the visual validation with OpenGL and GLSL using a modified ray-marching algorithm [15]. The fragment shader with our hard coded parametric representation of refractive index performs an iterative RK4 method [16] calculating the Refractive Radiative Transfer Equation until the ray hits a depth buffer. If the ray intersects with a depth buffer, a fragment for that ray becomes a color stored in that position of a color buffer. The parameters for the representation are then sent from CPU to GPU as the uniforms after the optimization, to visualize the optimization result. The number of iterations and the size of a step for RK4 can be adjusted to make a tradeoff between interactivity and precision.

We implemented a light ray visualizer inspired by the idea that Schmidt et al. [17] came up with. The trail of the light ray is visualized by series of points for every steps on 3D space, providing an important information of the light propagation in nonhomogeneous light media.

Chapter 6. Results

We present results from our system and renderer on a PC with Intel Core i7 3870 CPU with 3.6GHz, 16GB RAM, and NVIDIA GeForce GTX680 with 2GB of memory. We discuss various aspects of the results including the time required to solve the optimization problem, visual agreement to the desired goal, etc.

6.1 Optimization Time

The number of point pairs plays the prominent role on the performance, because the most costly operation during the optimization is calculating the light path. The average time increased from 1250 ms through 3864 ms, 5713 ms to 7750 ms for one, two, three, and four pairs of points, respectively (see Figure 6.1). The time increases as the number of point pair increases, because the total number of the light traces to be computed for every iteration is same as the number of point pairs.

6.2 Optimization and Rendering Results

We now present results of rendered images of mirage effects under the parameter settings we get from the optimization. Refer to Table 6.1 for the legend for the markers for understanding our UI and visualization of light traces.

Superior and inferior mirages. Figure 6.2 shows the optimization and rendering results for the superior mirage in the 3D scene. Note the location of the point pairs; there is the total of two pairs of points. One of them indicates a refraction result and, thus its trace of the light is curved, while its line of the sight is straight. On the other hand, two points of the other pair are set in the same position, representing not to be curved and thus acting as an anchor point; note that its trace of the light and the line of sight is aligned. We can visually check that the refraction visualization result proves that our method satisfies the goal state given by a user.

Figure 6.3 presents results for the inferior mirage in the 3D scene. Here, we used three pairs of points, two of which serves as anchor points above and under the refraction effect, which is given by the other pair, the middle pair in Figure 6.3-(b). The visualization result agrees on the user input here as well, showing that our method is available to handle generating both types of mirages.

Symbol	Description
Blue plus(+) sign	Destination point
Orange square(□) sign	Source point
Skyblue line	Line of sight
Yellow curve	Trace of light

Table 6.1: Legend for the markers in the screenshots

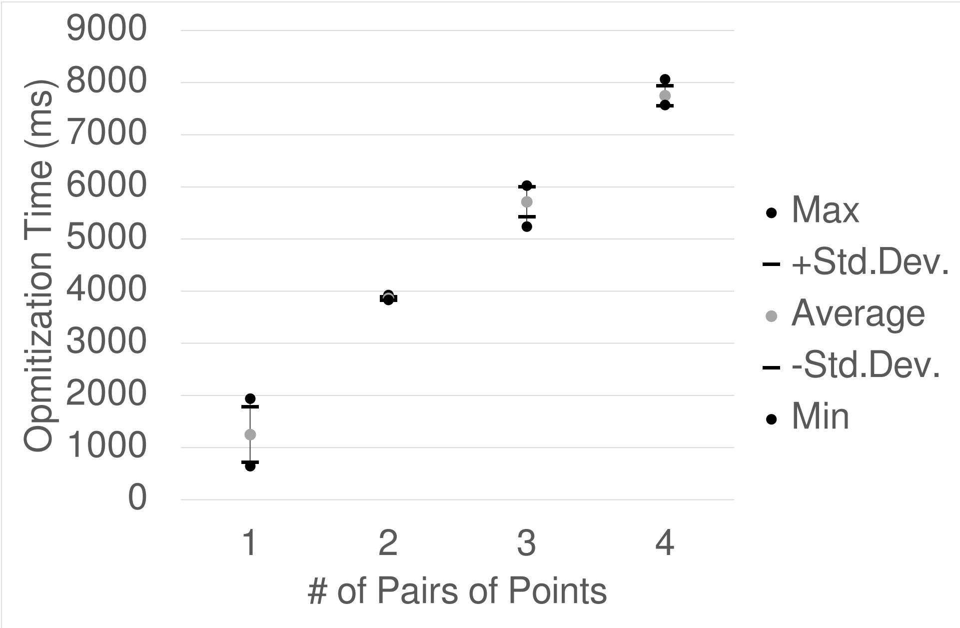

Figure 6.1: This shows the relationship between the number of Source-to-Destination Point Pairs and the time spent on optimization.

Different Distortions. Figure 6.4 also shows results for the inferior mirage in the 3D scene, but with the different distortion. Note the tighter user constraints, which are represented as three anchor point sets instead of two. The resulting rendered image agrees on the user input, which exhibits a tighter distortion than that of Figure 6.3.

The computed refractive index distribution allows interactive navigation of the scene. Figure 6.5 is the image of the same scene and refractive index setting as Figure 6.2, but with different camera setting. Because our method calculates the refractive index distribution not only just for the space inside the view frustum, but also for the whole scene, it is possible to navigate around the scene, while sharing the same atmosphere setting.

Our UI, refractive index representation, and optimization can be applied easily to 2D cases without any changes. Figure 6.6 shows results of 2D scenes created by our method.

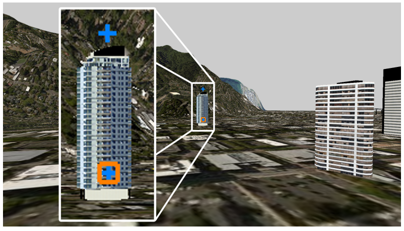

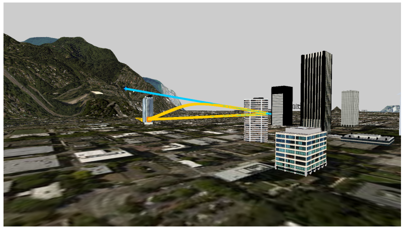

(a) Markers (user input) (b) Light traces

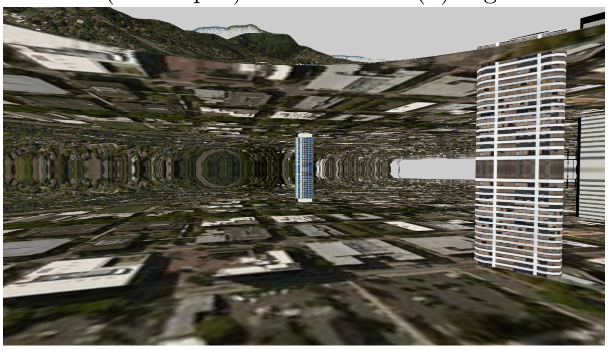

(c) Rendered image for a superior mirage

Figure 6.2: User input, light traces, and the rendered effect for a superior mirage in a 3D scene. User input is shown as marker; the blue plus (+) represents the destination point, and the orange square (□) represents the source point. The light traces acquired from the computed refractive index by the optimization is the visualized as the yellow curves, while the skyblue lines represent the line of sight; see Table 6.1 for the legend. The rightmost figure shows the computed mirage effect given the user input.

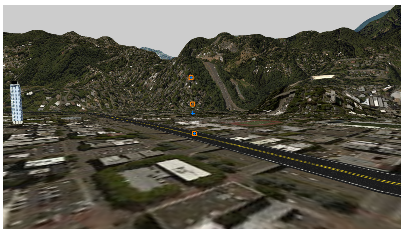

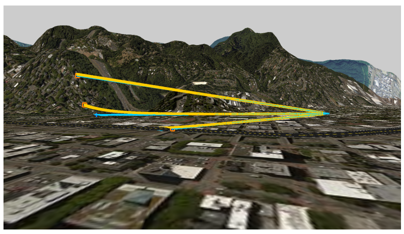

(a) Markers (b) Light traces

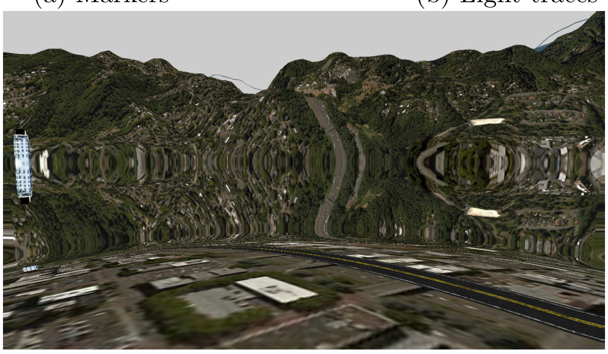

(c) Rendered image for an inferior mirage

Figure 6.3: The image (a) show user inputs, while the image (b) shows trace of lights. The image (c) shows the computed, inferior mirage effect.

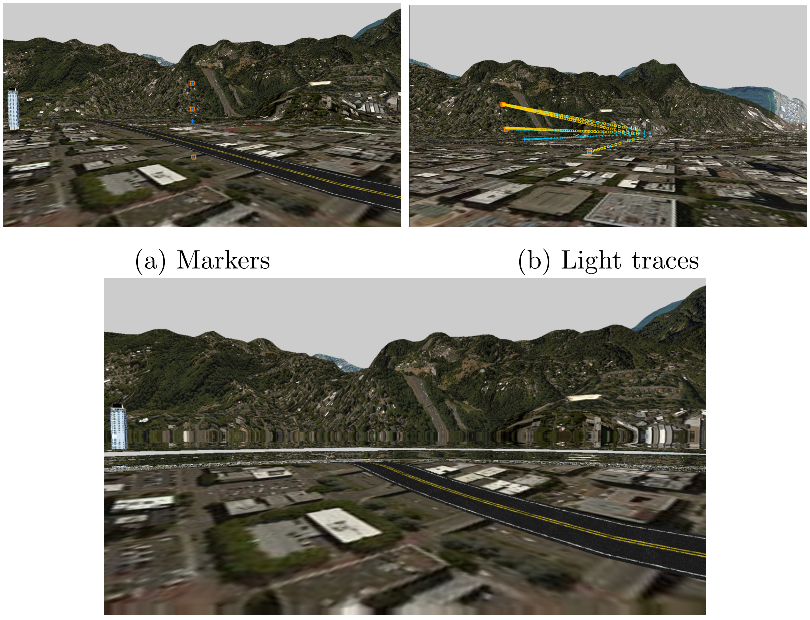

(a) Markers (b) Light traces

(c) Rendered image for an inferior mirage

Figure 6.4: The image (a) show user inputs, while the image (b) shows trace of lights. The image (c) shows the rendered inferior mirage effect. This one shows different distortion state compared to that of Figure 6.3.

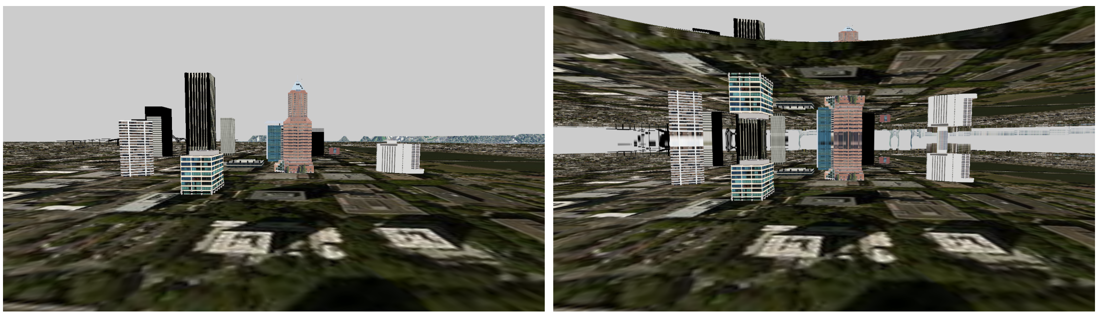

(a) Another location, without refraction (b) Same view direction as (a), with refraction

Figure 6.5: The image of the scene sharing the same refractive index settings as Figure 6.2. The image shows that the user can navigate through space with the consistent refractive index distribution.

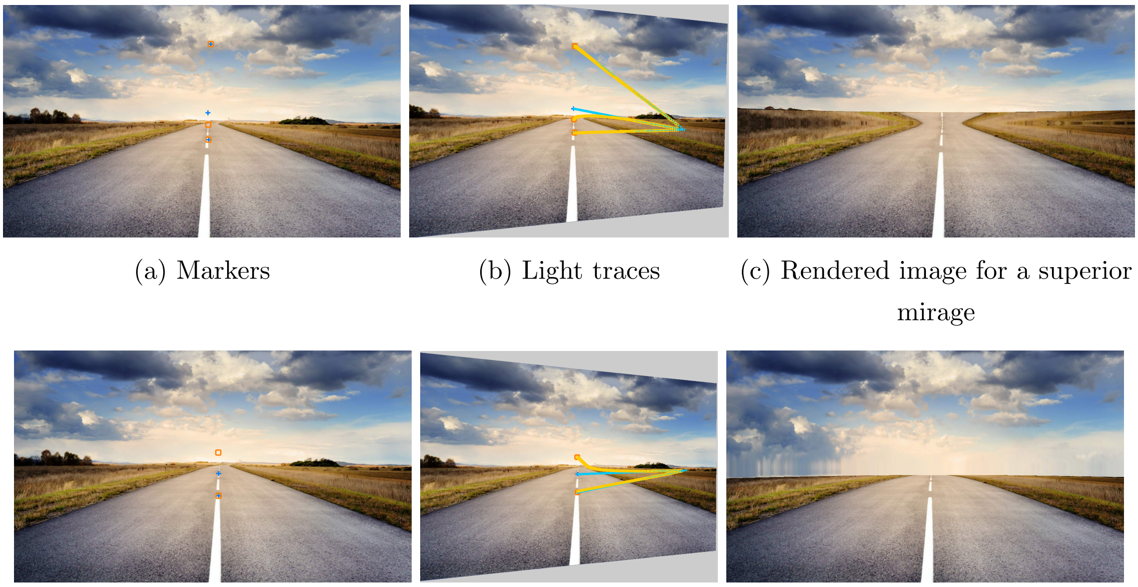

(a) Markers

(b) Light traces

(c) Rendered image for a superior mirage

(d) Markers

(e) Light traces

(f) Rendered image for a inferior mirage

Figure 6.6: This shows a 2D application for two different mirage types on 2D geometry. Our method can be easily applied to 2D scenes without any changes.

Chapter 7. Conclusion, Limitation and Future Work

We have introduced an intuitive user interface to control the appearance of a mirage effect, along with the appropriate parametric representation to encode a spatial distribution of a refractive index properly to be utilized in our method. The user interface gave a predictable control over mirage image generation, granting a user better artistic control. It was able to observe the model we suggested had a sufficient expression power to formulate the distribution of the refractive index for creating both types of mirages. Moreover, the time to optimize the solution based on given user inputs takes less than 10 seconds for up to four pairs of points, making each trial short enough to make an artistic editing session to be reasonably iterable.

Our method still has limitations. Since the system is computing the optimization based on the user constraints defined in the screen space rather than letting the user to directly modify the refractive index parameter, the system may not find convergence because the user constraints are not coherent to the model. In such case, the user may notice the problem visually through investigating an unwanted result they got and correct the constraints on their own via iteration of try and error. This is available thanks to the short time required to get an optimization done.

There are many interesting research directions. In this work, we have mainly looked at mirage effects as a function of the altitude. The model accompanying a difference along the other axis than the altitude can have better expression power and thus broaden the artistic control of mirage image generation. An extension to the user interface of Source-to-Destination Point Pairs is to adopt a ‘Source Region’ rather than a source point, updating the definition of the distance to the curve, and bringing more flexibility to an interface. Defining a region instead of a point may reduce the number of trials, where the system can have additional free space to move around, while satisfying the distance constraint between a region and a curve.

Bibliography

[1] M. Berger, N. Levit, T. Trout, and N. Analytical, "Rendering mirages and other atmospheric phenomena," in *Proceedings of EUROGRAPHICS'90*, pp. 459–468, 1990.

[2] D. Gutierrez, F. J. Seron, A. Munoz, and O. Anson, "Simulation of atmospheric phenomena," *Computers & Graphics*, vol. 30, no. 6, pp. 994–1010, 2006.

[3] Y. Zhao, Y. Han, Z. Fan, F. Qiu, Y.-C. Kuo, A. E. Kaufman, and K. Mueller, "Visual simulation of heat shimmering and mirage," *IEEE Transactions on Visualization and Computer Graphics*, vol. 13, no. 1, pp. 179–189, 2007.

[4] M. Ament, C. Bergmann, and D. Weiskopf, "Refractive radiative transfer equation," *ACM Transactions on Graphics (TOG)*, vol. 33, no. 2, p. 17, 2014.

[5] V. Holodovsky, Y. Y. Schechner, A. Levin, A. Levis, and A. Aides, "In-situ multi-view multi-scattering stochastic tomography," in *2016 IEEE International Conference on Computational Photography (ICCP)*, pp. 1–12, IEEE, 2016.

[6] E. Schrade, J. Hanika, and C. Dachsbacher, "Sparse high-degree polynomials for wide-angle lenses," in *Computer Graphics Forum*, vol. 35, pp. 89–97, Wiley Online Library, 2016.

[7] T.-W. Schmidt, F. Pellacini, D. Nowrouzezahrai, W. Jarosz, and C. Dachsbacher, "State of the art in artistic editing of appearance, lighting and material," in *Computer Graphics Forum*, Wiley Online Library, 2015.

[8] W. B. Kerr, F. Pellacini, and J. D. Denning, "Bendylights: Artistic control of direct illumination by curving light rays," in *Computer Graphics Forum*, vol. 29, pp. 1451–1459, Wiley Online Library, 2010.

[9] O. Klehm, I. Ihrke, H.-P. Seidel, and E. Eisemann, "Volume stylizer: Tomography-based volume painting," in *Proceedings of the ACM SIGGRAPH Symposium on Interactive 3D Graphics and Games*, pp. 161–168, ACM, 2013.

[10] T. Ritschel, M. Okabe, T. Thormählen, and H.-P. Seidel, "Interactive reflection editing," in *ACM Transactions on Graphics (TOG)*, vol. 28, p. 129, ACM, 2009.

[11] T. P. Dale and J. H. Gladstone, "On the influence of temperature on the refraction of light," *Philosophical Transactions of the Royal Society of London*, vol. 148, pp. 887–894, 1858.

[12] M. Born and E. Wolf, *Principles of optics: electromagnetic theory of propagation, interference and diffraction of light*. CUP Archive, 2000.

[13] M. J. Powell, "The bobyqa algorithm for bound constrained optimization without derivatives," *Cambridge NA Report NA2009/06, University of Cambridge, Cambridge*, 2009.

[14] L. M. Rios and N. V. Sahinidis, "Derivative-free optimization: a review of algorithms and comparison of software implementations," *Journal of Global Optimization*, vol. 56, no. 3, pp. 1247–1293, 2013.

[15] K. Perlin and E. M. Hoffert, "Hypertexture," in *ACM SIGGRAPH Computer Graphics*, vol. 23, pp. 253–262, ACM, 1989.

[16] W. H. Press, S. A. Teukolsky, W. T. Vetterling, and B. P. Flannery, *Numerical Recipes 3rd Edition: The Art of Scientific Computing*. 3 ed., 2007.

[17] T.-W. Schmidt, J. Novák, J. Meng, A. S. Kaplanyan, T. Reiner, D. Nowrouzezahrai, and C. Dachsbacher, "Path-space manipulation of physically-based light transport," *ACM Transactions On Graphics (TOG)*, vol. 32, no. 4, p. 129, 2013.

Acknowledgments in Korean

교육자로서, 선배 연구자로서, 연구실의 리더로서 많은 도움과 지도를 주신 지도교수님 윤성의 교수님께 감사드립니다. 교수님의 지도 하에 원하는 분야를 탐색하고 스스로가 흥미를 가질 수 있는 주제에 대해 연구할 수 있도록 전념할 수 있었습니다.

석사과정 기간 동안 함께할 수 있었던 모든 연구실 동료분들께 감사드립니다. 사회적으로 붙임성이 없는 성격임에도 불구하고 문제 없이 졸업할 수 있었던 데에는 연구실 동료분들의 깊은 배려심과 이해가 있었기에 가능했다고 생각합니다. 특히 동일 분야에서 연구 분야 탐색 및 조언에 도움을 주신 손명배님, 바쁘신 와중에도 프로젝트 진행 등에 있어 큰 도움을 주신 윤정수님, 연구 내용의 프리젠테이션에 도움을 주신 Pio님께 감사드립니다.

항상 무한한 믿음과 지원을 보내주시는 부모님께 감사드립니다. 믿음과 기대에 부응하기 위해 앞으로도 열심히, 즐겁게 살도록 하겠습니다.